

Particle shape effects on fabric of granular random packing



Shiwei Zhao^{a, b}, Nan Zhang^b, Xiaowen Zhou^{a, c, *}, Lei Zhang^b

^aSchool of Civil Engineering and Transportation, South China University of Technology, Guangzhou 510640, China

^bSchool of Civil and Construction Engineering, Oregon State University, Corvallis 97333, USA

^cPowerchina Huadong Engineering Corporation Limited, Hangzhou 310014, China

ARTICLE INFO

Article history:

Received 2 October 2016

Received in revised form 28 December 2016

Accepted 31 December 2016

Available online 4 January 2017

Keywords:

Discrete element method

Random packing

Superellipsoids

Fabric

Particle shape

Anisotropy

ABSTRACT

A numerical investigation of particle shape effects on fabric of granular packing is carried out using the three dimensional discrete element method with a superellipsoid model. A broad range of particle shapes controlled by two shape parameters (i.e., aspect ratio and blockiness) are taken into account. A series of random packing of non-cohesive, frictional monodisperse superellipsoids is conducted under gravitational forces in simulations. Fabric of a granular packing is quantified in terms of packing density, coordination number, distribution of particle orientations, anisotropy of three types of fabric vectors (i.e., particle orientation, contact normal and branch vector), and distribution of normalized contact forces. It is shown that the effects of particle shape on packing density and mean coordination number are in agreement with the reported in the literature. Moreover, ellipsoids show the lowest packing density in the family of superellipsoids. The distribution of particle orientations is much more sensitive to blockiness than aspect ratio. It is also found out that anisotropy of both particle orientations and contact normals shows a similar M-type relationship with aspect ratio, two times larger than that of branch vectors. Interestingly, particle shape has an insignificant effect on the probability distribution of normalized contact forces which shows a clear exponential distribution. Those findings would be useful for a better understanding of the initial fabric of granular packing, especially in granular mechanics and geomechanics.

© 2017 Elsevier B.V. All rights reserved.

1. Introduction

Random packing of granular materials is ubiquitous in nature and industry. Their interesting structural properties have been the focus of a considerable body of research [1–4]. In laboratory, some basic shapes, e.g., spheres [5–7], ellipsoids [8] and regular convex polyhedra [4,9], have been used to investigate packing properties. However, such experiments are extremely laborious and even expensive. Moreover, it is not straightforward to obtain the microscopic information of a packing for a better understanding. Therefore, many researchers prefer to conduct numerical simulations instead. There are several available numerical methods, e.g., the discrete element method (DEM) [10], Monte Carlo simulations [11], the Lubachevsky-Stillinger algorithm [12] and molecular dynamics [13]. To the best of our knowledge, DEM is the most popular due to its power of simulating physical process in real life. The reader is referred to the

literature [14] for a good review of DEM applications on granular systems.

Particle shape has a significant effect on a packing structure [9,15–17]. Packing of non-spherical particles has considerably different properties from that of spherical particles [18]. In recent years, extensive numerical investigations on packing of non-spherical particles were carried out. For example, Lu et al. [19] and Kyrylyuk and Philipse [16] investigated the relationship between packing density and aspect ratio using spherocylinders. Deng and Davé [20] used the multi-sphere method to investigate the effect of the particle size, aspect ratio on the packing of spherocylinders. Nan et al. [21] investigated random packing of rigid fibers with variable aspect ratio and curvature using a multi-sphere model. Li et al. [18] reported the maximum random packing densities of basic three-dimensional shapes using sphere assembly models. Zhou et al. [22] simulated the random packing of ellipsoidal particles, and reported that the maximum packing density occurs at an aspect ratio of 0.6 for oblate spheroids, and 1.8 for prolate spheroids, qualitatively in agreement with the results of Donev et al. [8]. Following Zhou et al. [22], Gan et al. [23] conducted packing simulations of ellipsoids by considering the presence of the van der Waals force between fine particles. For polyhedral shapes, Jiao and Torquato [24] investigated

* Corresponding author at: School of Civil Engineering and Transportation, South China University of Technology, Guangzhou 510640, China.
E-mail address: xwzhou@scut.edu.cn (X. Zhou).

the effect of particle shape on packing density using the adaptive-shrinking-cell method [25]. In particular, the regular tetrahedron has the lower bound [26] and upper bound [4] of packing density among convex polyhedra; it also has the upper bound of packing density in the family of tetrahedra [27,28]. Most of the literature mentioned above focused on the two packing descriptors, i.e., packing density and coordination number. However, these two descriptors are not sufficient to give a deeper insight into fabric of a granular packing.

Fabric of a granular packing (or assembly) is the arrangement of the particles, i.e., the topology of the internal structure of the packing [29], which has considerable effects on the macroscopic properties of the packing [30–32]. Especially in granular mechanics and geomechanics, previous investigations show that the initial fabric of a granular material has a significant effect on the mechanical behaviors [30,31,33,34]. For quantitative studies, fabric can be quantified using several measures, e.g., packing density, the coordination number, the distribution of particle orientations, the distribution of contact normals, and the distribution of branch vectors [29]. In addition, local voids around individual particles are attractive as well. Oda [35] first quantified the local porosity distribution for sands in 2D by connecting the mass centers of particles surrounding a void to define a polygonal cell. A better alternative of Oda's method is the Voronoi tessellation (i.e., the so-called Voronoi analysis), which is able to more precisely characterize the local void. This method has been widely applied to sphere packings, e.g. [36], including an extension, radical Voronoi (i.e., Laguerre) tessellation, for granocentric models [37,38], whereas just a few for non-spherical particles [39–42] due to the complication of construction of Voronoi cells. To date, few investigations on the fabric of random packing of granular materials were reported. In this work, we focus on the initial fabric of a granular packing, i.e., the fabric after packing.

Superellipsoids are able to capture many of the essential features of real particle shapes [43] and represent a wide range of shapes in nature [44]. Superellipsoids-based DEM has been applied to simulating granular flows in industry [45]. In this work, a DEM model based on superellipsoids is developed and embedded into the open-source DEM code, YADE [46,47]. Using the present model, we conduct a series of random packing of superellipsoids with a broad range of particle shapes under a gravitational field, analogous to the formation of a sand pile in nature. Effects of particle shape on packing density and coordination number are investigated first, followed by probability distributions of particle orientations. For a further understanding of fabric, anisotropy of fabric vectors and probability distributions of normalized contact forces are analyzed.

2. Discrete element model

2.1. Superellipsoids

The surface function of a superellipsoid in the local Cartesian coordinates can be defined as [48]

$$\left(\left| \frac{x}{a} \right|^{\frac{2}{\epsilon_1}} + \left| \frac{y}{b} \right|^{\frac{2}{\epsilon_2}} \right)^{\frac{\epsilon_1}{2}} + \left| \frac{z}{c} \right|^{\frac{2}{\epsilon_3}} = 1 \quad (1)$$

where a , b and c are referred to be the semi-major axis lengths in the direction of x , y , and z axes, respectively, and ϵ_i , ($i = 1, 2$) are the shape parameters determining the sharpness of particle edges. The interested reader is referred to [43,44] for other similar definitions of a superellipsoid. The present work focuses on convex shapes whose corresponding ϵ_i is in $(0, 2)$. Changing ϵ_i gives a wide ranges of shapes (see Fig. 1). In particular, $\epsilon_i \rightarrow 0$ gives a cubic shape, while $\epsilon_i \rightarrow 2$ corresponds to an octahedral shape. Appendix A gives a series of important geometric properties of a superellipsoid involved in the present model.

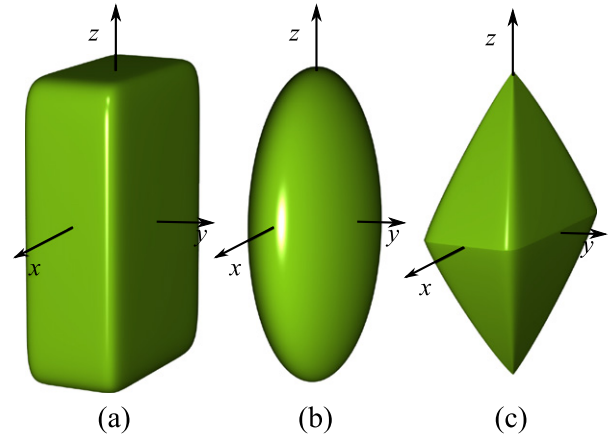


Fig. 1. Superellipsoids with $a = 2$, $b = 1$, $c = 3$ and (a) $\epsilon_1 = \epsilon_2 = 0.2$, (b) $\epsilon_1 = \epsilon_2 = 1.0$, and (c) $\epsilon_1 = 0.2$, $\epsilon_2 = 1.8$.

2.2. Equations of motion

Particle motion can be decomposed into two parts: translation and rotation. The translation of a particle is governed by Newton's equations:

$$m \frac{dv_i}{dt} = F_i \quad (2)$$

where $i \in 1, 2, 3$ is the global coordination axis; m is the mass, given by Eq. (A.1); v_i is the translational velocity, and F_i is the resultant force acting on the centroid.

Meanwhile, Euler's equations are applied for particle rotation:

$$I_i \frac{d\omega_i}{dt} - (I_j - I_k)\omega_j\omega_k = M_i \quad (3)$$

where $i \in 1, 2, 3$ is the principal axis and i, j, k are subsequent indexes; I_i is the principal moment of inertia, given by Eq. (A.3); ω_i is the angular velocity, and M_i is the resultant torque around the centroid.

Newton's and Euler's equations are solved, respectively, using the standard and the extending leapfrog algorithm [49]. Following general DEM codes, artificial numerical damping is used to dissipate kinetic energy in the system. Thus, a corresponding damping force $f^{(d)}$ is added to the right-hand of Eqs. (2) and (3), given as [47]

$$f_i^{(d)} = -\alpha F_i \text{Sign} \left(F_i \left(v_i^{(t-\Delta t/2)} + \frac{dv_i^t}{dt} \frac{\Delta t}{2} \right) \right), i \in \{1, 2, 3\} \quad (4)$$

where α is the damping coefficient; Δt is the time step, $v_i^{(t-\Delta t/2)}$ the previous mid-step velocity, $\frac{dv_i^t}{dt}$ the current on-step acceleration, $\text{Sign}(x)$ the signum function (see Eq. (A.6)).

2.3. Contact force law

The present DEM is based on the soft particle method [10], where particles are allowed to overlap, referring to Fig. 2. As a consequence, repulsive force can be calculated from the overlap in terms of a given model. There are a wide range of available models. However, for simplicity, a common linear spring model [50] is used in this work, given as follows.

$$\begin{cases} F_n = \delta K_n \\ F_t = \min \{ F_t' + \Delta u K_t, \mu F_n \} \end{cases} \quad (5)$$

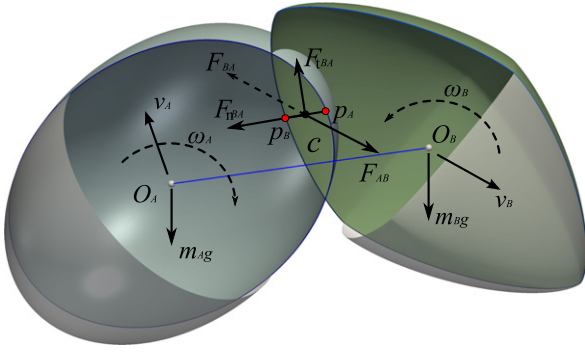


Fig. 2. Three-dimensional illustration of two touching particles. The size of the overlap region is exaggerated for clarity.

where F_n and F_t are the normal and tangential contact forces, respectively; K_n and K_t are their corresponding normal and tangential contact stiffness; Δu is the contact incremental displacement at each time step while δ is the penetration depth of entities at contact; μ is friction coefficient; F_t' is the tangential contact force at the previous time step. Note that the Coulomb condition (or sliding friction model) is applied to tangential contact force. The tangential contact force F_t' is initialized to zero when the contact is formed. The contact stiffness K_* (* representing n or t) is set to the harmonic mean of the stiffness of the two entities at contact, given by Eq. (6), where the subscripts A and B denote the two particles in contact.

$$K_* = \frac{2K_*^A K_*^B}{K_*^A + K_*^B} \quad (6)$$

2.4. Geometric quantities at contact

The penetration depth and the contact direction are updated for the calculation of contact forces at each time step. Given two adjacent particles A and B, the potential contact points, denoted as \mathbf{p}^A and \mathbf{p}^B from each particle, yield a potential contact penetration $\mathbf{d} = (\mathbf{p}^B - \mathbf{p}^A)$, referring to Fig. 3 (a). Based on the common-normal concept [51,52], the desired contact points make the penetration depth minimum and subjected to the following conditions:

- (1) the unit vectors, \mathbf{n}^A and \mathbf{n}^B , of the outward surface normals at \mathbf{p}^A and \mathbf{p}^B are parallel and anti-parallel to the contact direction \mathbf{c} , respectively:

$$\mathbf{n}^A = -\mathbf{n}^B = \mathbf{c} \quad (7)$$

- (2) the potential contact penetration \mathbf{d} is parallel to the contact direction \mathbf{c} :

$$\mathbf{d} \times \mathbf{c} = \mathbf{0} \quad (8)$$

Therefore, finding the contact points is an optimization problem. As suggested by Wellmann et al. [52], the contact direction \mathbf{c} is parameterized by two angles in a local spherical coordinate system, i.e.,

$$\mathbf{c}(\alpha, \beta) = \cos \alpha \cos \beta \mathbf{i} + \sin \alpha \cos \beta \mathbf{j} + \sin \beta \mathbf{k} \quad (9)$$

where \mathbf{i} , \mathbf{j} , and \mathbf{k} are unit base vectors of the global Cartesian coordinate system. Consequently, considering Eq. (7), the contact points are expressed as

$$\begin{cases} \mathbf{p}^A = \mathbf{T}_A^{-1} F^A(f^A(\mathbf{T}_A \mathbf{c}(\alpha, \beta))) + \mathbf{s}^A \\ \mathbf{p}^B = \mathbf{T}_B^{-1} F^B(f^B(-\mathbf{T}_B \mathbf{c}(\alpha, \beta))) + \mathbf{s}^B \end{cases} \quad (10)$$

where \mathbf{T} is the rotation matrix of a particle from the global coordinate system to the local, and \mathbf{T}^{-1} is its inverse; \mathbf{s} is the position vector of a particle; f and F are two geometric functions at the local of a particle (see Eqs. (A.5) and (A.7)). Therefore, finding the penetration depth $\|\mathbf{d}\|$ becomes the following unconstrained optimization problem with two parameters:

$$\min_{\alpha, \beta} \|\mathbf{d}\| = \min_{\alpha, \beta} \|\mathbf{p}^B - \mathbf{p}^A\| \quad (11)$$

The Nelder-Mead simplex algorithm [53] is adopted to obtain a robust solution. It is worth noting that Eq. (8) is fulfilled when Eq. (11) reaches a global minimum [52].

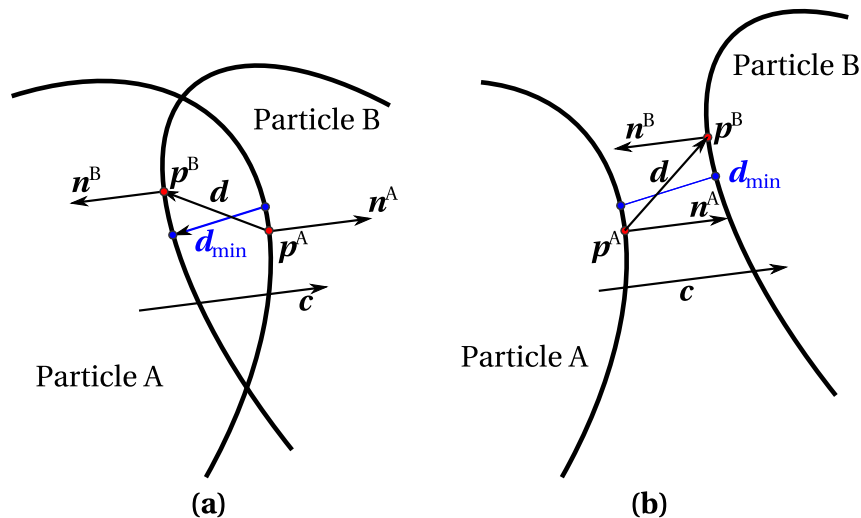


Fig. 3. Two-dimensional schematic of the optimization solving between two (a) touching and (b) non-touching particles.

2.5. Contact detection

Given that so many particles need collision detection at each time step, a combination of approximate collision detection and exact detection is applied to reducing the computational cost. A two-level approximate collision detection scheme is provided. At the first level, the AABB (axis-aligned bounding box) algorithm [54] is used to rule out most of the particles that are not touching one another. For the special case of superellipsoids, we use a fixed-size cubic AABB for each particle. Then, spherical bounding boxes are used for a further sweep at the second level. For the rest particles potentially in contact, the exact detection is undertaken, which is introduced in Section 2.4. During the optimization solving, it is useful to check the following condition at each iteration.

$$\mathbf{d} \cdot \mathbf{c} > 0 \quad (12)$$

If this condition is true, particles are not touching [52], referring to Fig. 3 (b). Therefore, we can rule out the current particle pair and terminate the detection.

3. Simulation setup

3.1. Particle shapes and properties

The present DEM model is able to model shapes with the whole range of superellipsoids determined by five shape-related parameters (i.e., a, b, c, ϵ_1 and ϵ_2) as shown in Eq. (1). However, studying the whole range of shapes is a huge work and needs significantly high computational cost. We, thus, focus on the cases with $a = b = \eta c$ and $\epsilon_1 = \epsilon_2 = \zeta$, where η is aspect ratio, and ζ is referred to as blockiness [55,56]. Fig. 4 shows some shapes used in the simulations.

Particle properties used in the simulations are given in Table 1. Particle size r is the radius of a sphere with equivalent volume. The particle density ρ and the inter-particle sliding friction coefficient μ correspond to that of natural sand measured in laboratory [57]. Walls of the container are frictionless with the same stiffness as particles. The values of the other parameters are selected from the literature. It is worth pointing out that there is not a theoretical critical time step for a non-spheres system. Hence, the present time step is selected tentatively based on empirical trials and values in the literature to make simulations numerically stable.

3.2. Packing procedure

A packing can be formed under different conditions, such as pouring or tapping, sequential addition, and vibration [9,22]. Given that this work mainly focuses on natural depositing of particles under a gravitational field, the sequential addition method is applied. In

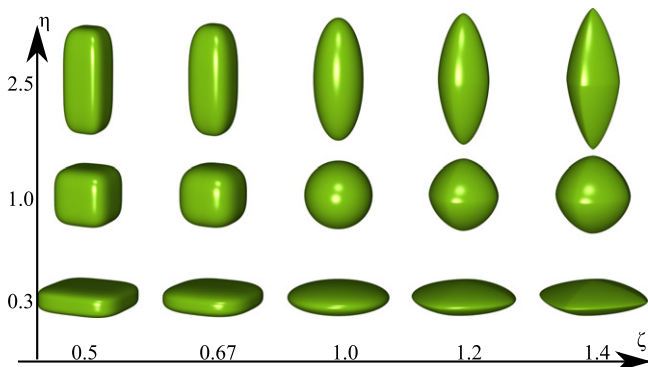


Fig. 4. Examples of shapes used in the simulations.

Table 1

Particle parameters used in the DEM simulation.

Parameter	Value
Particle size, r (mm)	10
Particle aspect ratio, η	0.3 ~ 2.5
Particle blockiness, ζ	0.5 ~ 1.4
Particle density, ρ (kg/m^3)	2650
Coefficient of friction, μ	0.48
Damping coefficient, α	0.3
Particle normal stiffness, K_n (N/m)	1×10^7
Particle shear stiffness, K_t (N/m)	7×10^6
Time step, Δt (s)	5×10^{-6}

detail, non-overlapping particles are added layer by layer into a cubic container with a dimension of $350\text{mm} \times 350\text{mm} \times 1000\text{mm}$. Each layer consists of 50 particles with random locations and orientations, and is added to the container from a height of five times the particle size every 0.05 s. Each packing is made up of 5000 monodisperse particles. For 60 particle shapes controlled by 12η and 5ζ , 60 simulations in total are carried out. For each simulation, it takes around 120 h on a 3.4 GHz Xeon CPU in average to reach an assumed equilibrium state, where the average particle velocity is less than 1×10^{-4} m/s. Fig. 5 shows some final packings for an initial observational comparison.

4. Results and discussion

4.1. Packing density

Packing density (fraction) and coordination number are two of the commonly used parameters describing the structure of a packing [58,59]. Packing density is defined as ratio of the solid volume to the total packing volume including voids. Given that the top free surface of a packing is not regular, an imaginary cubic box with the same bottom as the container (hereafter referred to as the measurement box) is introduced to measure the packing density. Consequently, the solid is made up of all particles with centroids inside the measurement box, and the total packing volume is equal to the box volume. For a more accurate measurement, one hundred measurement boxes with heights uniformly distributed between 150 mm and 200 mm are generated. The average of one hundred corresponding packing densities, then, is taken as the final packing density.

Fig. 6 shows relationship between packing density and aspect ratio for ellipsoidal particles ($\zeta = 1$). It can be seen that there is a peak at an aspect ratio of near 0.6 for oblate ellipsoids ($\eta < 1$), and a peak at an aspect ratio of near 1.5 for prolate ellipsoids ($\eta > 1$). Such an M-type trend in packing density with aspect ratio is in good agreement with other DEM results in the literature [8,22,60]. Quantitatively, the results of Donev et al. [8] and Delaney and Cleary [60] are larger than those of Zhou et al. [22] and this work, especially near the two peaks, due to different packing methods applied. Donev et al. [8] and Delaney and Cleary [60] used the Lubachevsky-Stillinger algorithm (LS) [12] by which particles expand with a growing rate, whereas Zhou et al. [22] and this work used the particle depositing method by which particles free deposit under gravitational forces. The reader is referred to the literature [22] for a more detailed comparison between these two methods. In addition, it is worth mentioning that the parameter values of material properties in these work are not quantitatively consistent with one another, thereby causing some discrepancies in the results to some extent.

For superellipsoids with aspect ratio $\eta = 1$ (i.e., so-called superballs), variation in packing density with blockiness ζ is shown in Fig. 7. It is observed that spherical particles ($\zeta = 1$) have the lowest packing density of around 0.62, which is lightly below the RCP

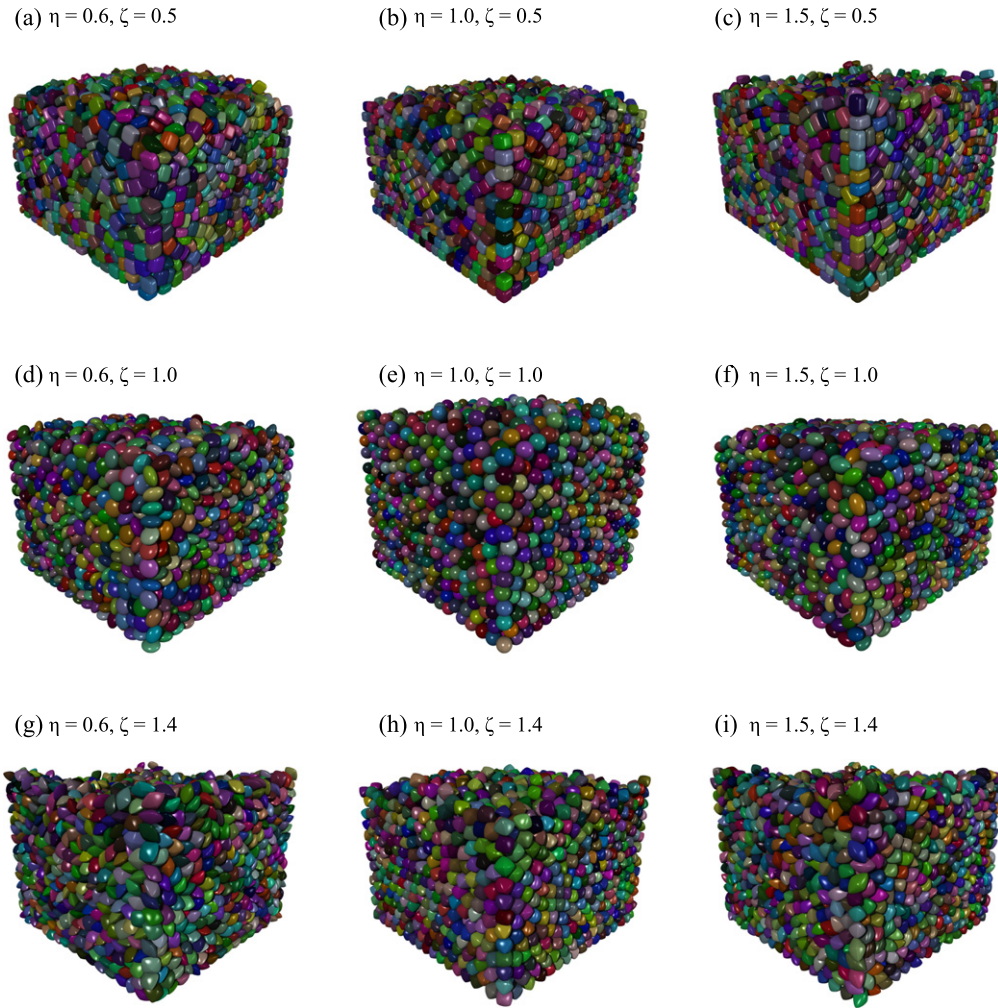


Fig. 5. Packings of superellipsoids with different blockiness ζ and aspect ratio η .

density limit of $\phi \simeq 0.64$ in frictionless systems. Changing blockiness ζ away from 1.0, packing density increases. This feature was reported by Jiao et al. [61] and Delaney and Cleary [60] as well, whose results are replotted together in Fig. 7 to make a comparison. It is worth pointing out that Jiao et al. [61] shows the upper-bound packing density where particles place in the lattice packing.

Results of the two special cases (i.e., ellipsoids and superballs) are qualitatively consistent with the literature, even though packing methods and model parameters adopted are somewhat different, indicating that the present DEM model is reasonable. Some further simulations are undertaken with a wide range of particle shapes for superellipsoids varying blockiness ζ and aspect ratio η .

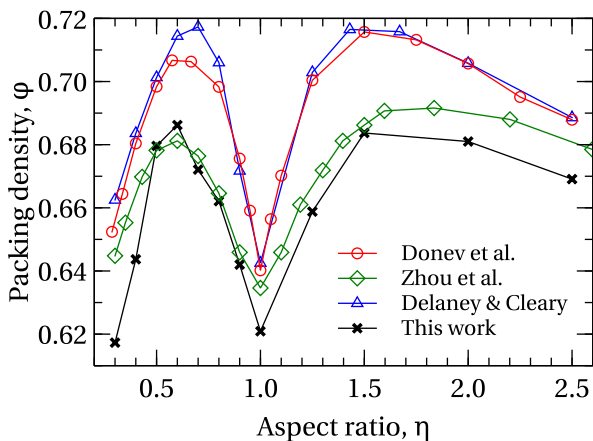


Fig. 6. Relationship between packing density and aspect ratio for ellipsoids.

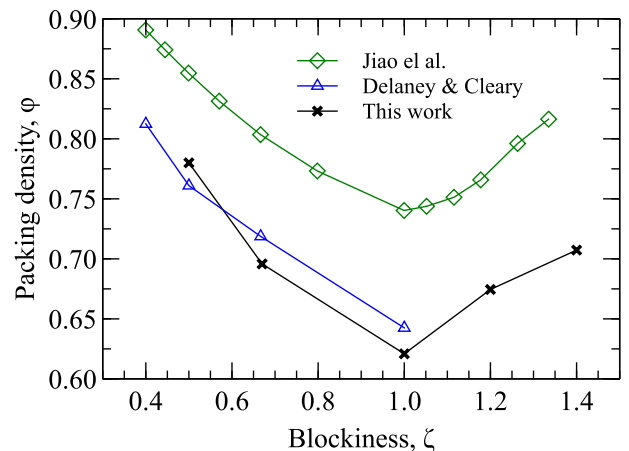


Fig. 7. Variation in packing density with blockiness ζ for superballs.

Fig. 8 shows relationships between packing density and aspect ratio η with different blockiness ζ . For a given blockiness ζ , relationship between packing density ϕ and aspect ratio η shows two types of trends: one is M-type with two peaks at $\eta \approx 0.6$ and $\eta \approx 1.5$, and the other is inverted V-type with one peak at $\eta = 1.0$. For blockiness ζ decreasing from 1.0, the ϕ - η curve moves up seeing a M-type transferring to an inverted V-type trend. A similar trend was observed in Delaney and Cleary [60]. Moreover, for blockiness ζ increasing from 1.0, the ϕ - η curve behaves in a similar fashion. Overall, ellipsoids have the lowest packing density in the family of superellipsoids.

4.2. Coordination number

Coordination number(CN), defined as the number of particles in contact with a considered particle, is an important quantity for the quantification of internal structural features (i.e., fabric) of a granular packing. As a meso-scale parameter, coordination number pronounces louder in macroscopic properties than packing density of a granular packing. For example, Agnolin and Roux [62] showed that the bulk moduli are primarily sensitive to coordination number instead of packing density, as is conventionally believed. In the present study, it is assumed that two particles touch one another if there is an overlap between them, i.e. that the normal contact force is non-zero in terms of the given contact model.

Fig. 9 shows the dependence of the mean coordination number Z with aspect ratio η for ellipsoids. It can be seen that as the aspect ratio η increases or decreases from 1.0, the mean coordination number increases to reach a peak then slowly decreases. This trend qualitatively agrees with that in the literature [8,22,60]. Compared with the variation of packing density in Fig. 6, it is found out that a high mean coordination number is not corresponding to a high packing density due to the effect of aspect ratio [22,28]. Such a phenomenon occurs with varying blockiness. Take cubic-like shapes with $\zeta = 0.5$ as an example, the particle shape at $\eta = 1.0$ sees the highest packing density but the lowest coordination number. The main reason is

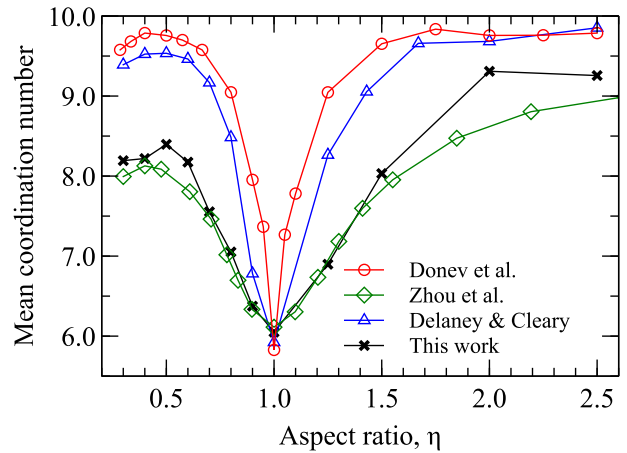


Fig. 9. Variation in mean coordination number Z with aspect ratio η for ellipsoids.

that particles with $\eta = 1.0$ are more likely to form face-face contacts, referring to Fig. 5 (a)–(c) for an observational comparison. Furthermore, with varying blockiness ζ , the Z - η curve behaves in a similar fashion, referring Fig. 10, which is consistent with the literature [60]. In addition, the effects of blockiness ζ on both packing density and mean coordination number are significant at aspect ratios near 1.0.

It is worth noting that a clear correlation between packing density and mean coordination number was observed in sphere packings. For non-sphere packings, it can be also seen that packing density is positively related to mean coordination number by varying the external conditions from the same initial packing structure (i.e., initial fabric), e.g., varying the loading on the packing [63], or by changing material properties, e.g., varying inter-particle coefficient of friction [22]. However, changing the particle shape is likely to significantly affect the initial structure, thereby resulting in an unclear relationship

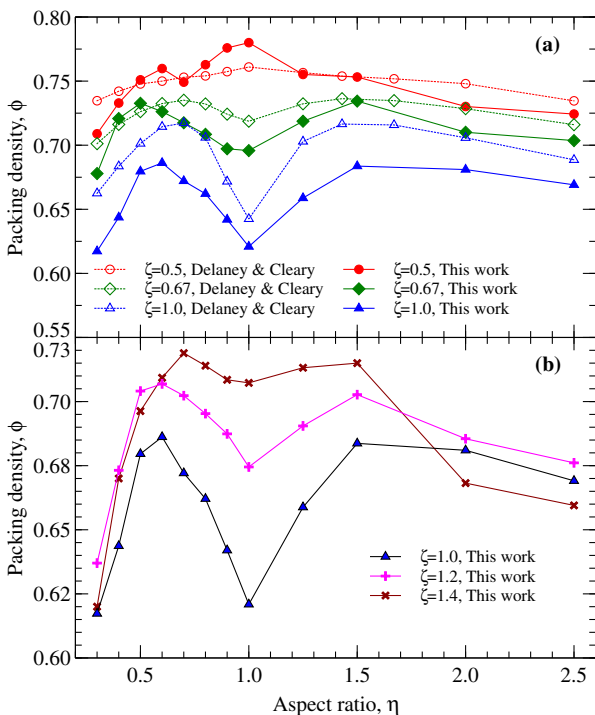


Fig. 8. Relationships between packing density and aspect ratio η for superellipsoids with different blockiness ζ .

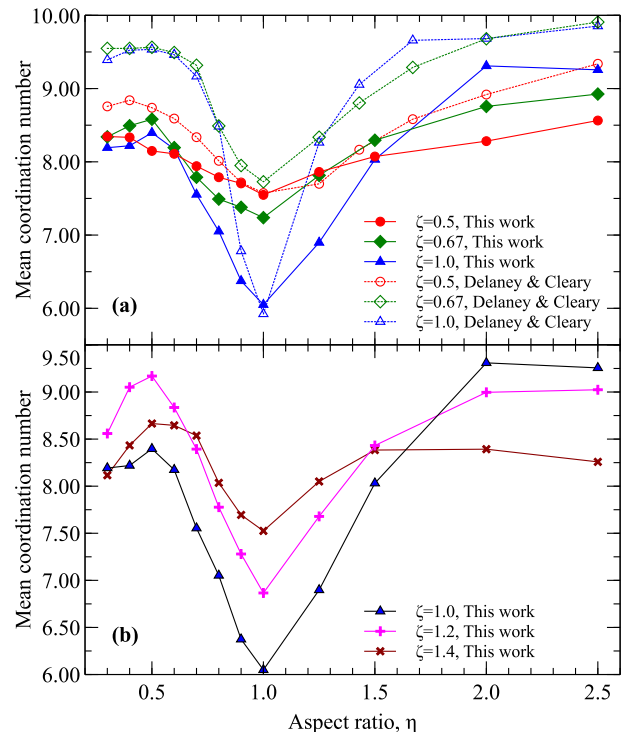


Fig. 10. Variation in mean coordination number Z with aspect ratio η for superellipsoids.

between packing density and mean coordination number for different particle shapes. That is the case in the present study.

A probability distribution of coordination number is one measure of anisotropy of scalar-based fabric within a granular packing. More analysis of anisotropy is conducted in the following sections. Fig. 11 shows probability distributions of coordination number for superellipsoids with different blockiness ζ and aspect ratio η . The curves are well described by Gaussian distributions, although there seems to be some systematic skewness at the tails. The distribution moves to the right as aspect ratio decreases or increases from 1.0 for a given blockiness, corresponding to an increasing mean coordination number in Figs. 9 and 10, and implying that anisotropy increases. However, the distribution is likely to move to the left when the shape becomes sufficiently oblate or prolate. Interestingly, the peak of distribution varies at a range of aspect ratios between 6.1 and 9.0. Moreover, as blockiness ζ increases or decreases from 1.0, the range appears to be narrower, e.g., [7.6, 8.5] at $\zeta = 0.5$, suggesting that anisotropy decreases. With respect to superballs ($\eta = 1.0$), the distribution moves to the right with ζ increasing or decreasing from 1.0.

4.3. Distribution of particle orientations

Previous investigations show that bulk properties of a granular material are significantly related to the distribution of particle orientations. For example, the stress-strain relationship and shear strength have been found to depend on the direction of loading with respect to the direction of particle orientation [30,31,33,34]. Effects of particle shape on the distribution of particle orientations within a granular packing are quantitatively investigated in this section. It is assumed that the orientation of a particle is along its long axis. Given that the interpretation of a three-dimensional distribution of particle orientations is difficult, we project particle orientations on the horizontal and vertical planes for ease of visualization, referring to Fig. 12. Note that no data for particle orientations of superballs ($\eta = 1$) are presented due to unavailable definitions for a superball orientation in terms of the present definition.

As shown in Fig. 12, the distribution of particle orientations on the horizontal plane is much more uniform than that on the vertical plane. Moreover, major particles have orientations along near the

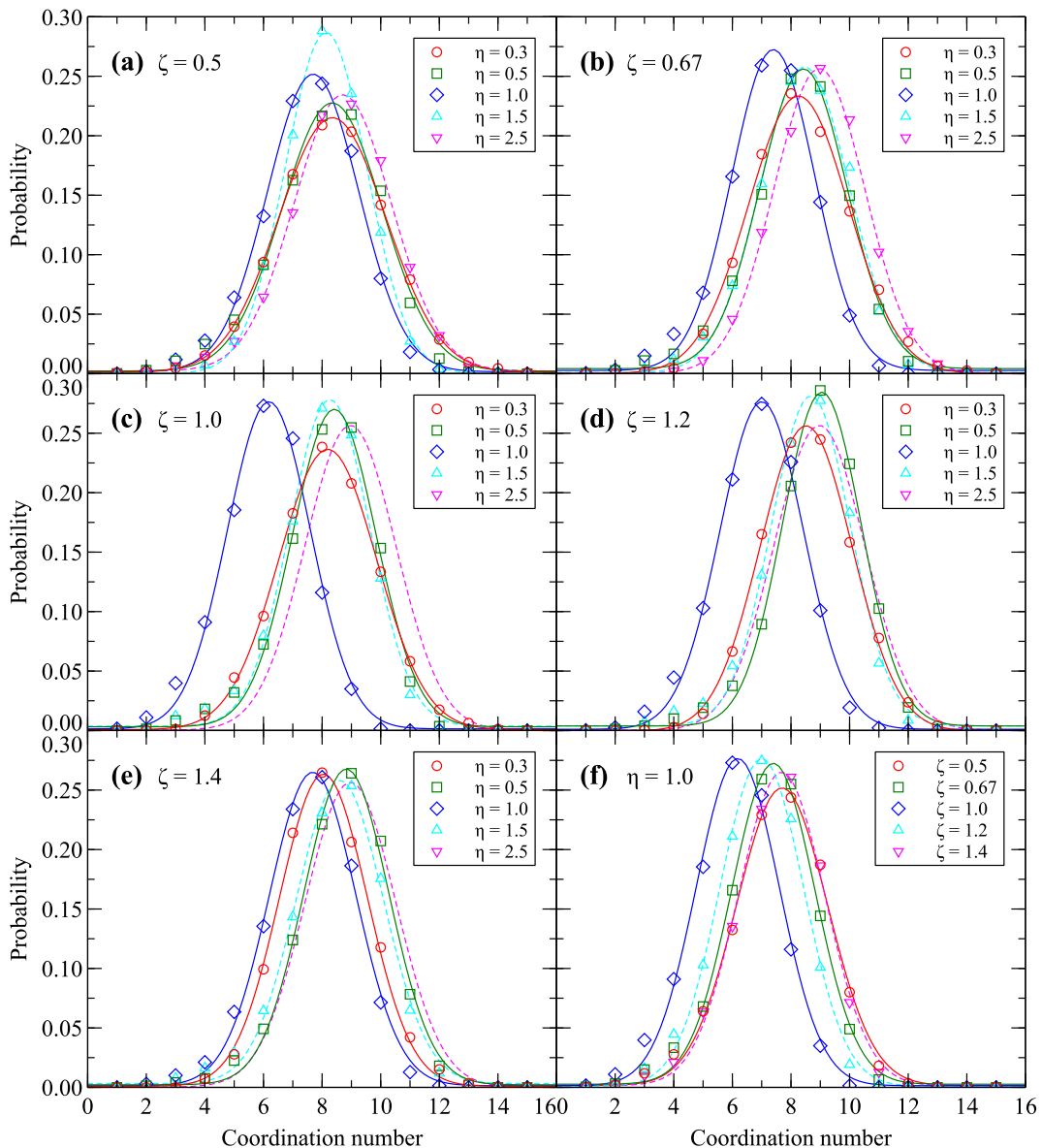


Fig. 11. Effects of aspect ratio η ((a)–(e)) and blockiness ζ (f) on probability distribution of coordination numbers for superellipsoids. The curves are fits to Gaussian distributions.

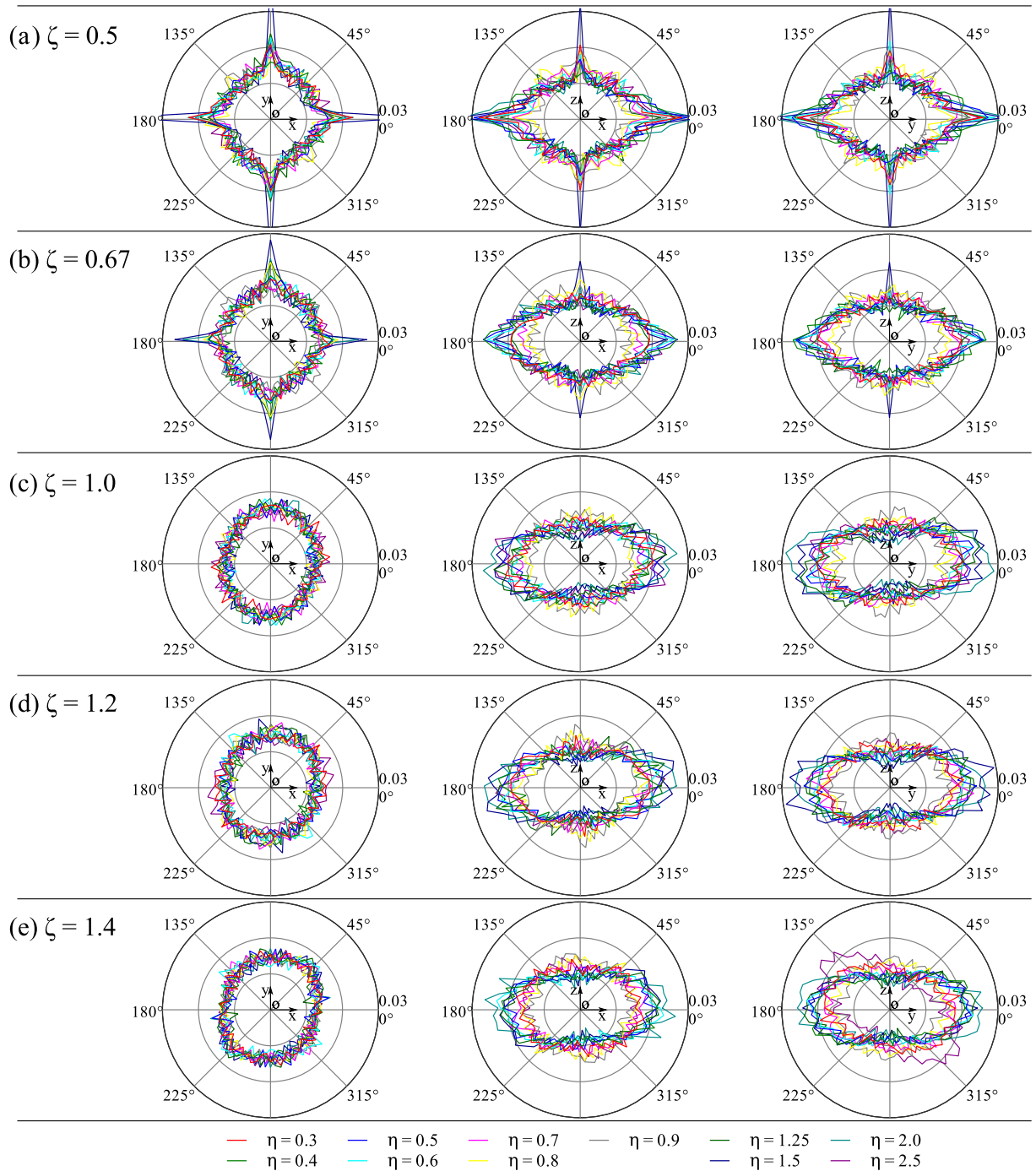


Fig. 12. Probability distributions of particle orientations projected on the horizontal (the left column) and vertical (the middle and right columns) planes for different blockiness ζ and aspect ratio η .

horizontal plane. That is because a particle is more likely to align along the long axis to reach a stable state during depositing. For the effect of aspect ratio η on the particle orientation, it is significant on the vertical plane, but not on the horizontal plane. As expected, the distribution tends to form a circle with $\eta \rightarrow 1$. That is to say, it is more possible for a particle with a longer axis to align near the horizontal plane. However, such a trend disappears when particles are sufficiently oblate or prolate. For instance, the distribution of particle orientation is likely to become more uniform with η decreasing from 0.5 or increasing from 2.0 or increasing from 2.0 in Fig. 12 (c).

Compared with aspect ratio η , blockiness ζ has much more dramatic effects on the distribution of particle orientations. For $\zeta = 1.0$, a circle-like distribution is observed on the horizontal plane, an ellipse-like distribution on the vertical plane. As ζ decreases from 1.0, the distribution is likely to become more square-like on the horizontal plane, and parallelogram-like on the vertical plane. By contrast, increasing ζ from 1.0, the distribution on the horizontal plane tends to a square but not significantly as the cases of $\zeta < 1.0$. However, on the vertical plane, the distribution sees a small change. The reason why ζ has such a significant effect on these diagrams is noted here.

Changing ζ away from 1.0, the sharper edges of particles come out and the particle faces become more flat, thereby increasing face-face contacts forming columnar phases, referring to Fig. 5 for an observation. Furthermore, considering two extreme cases, cubic particles ($\zeta \rightarrow 0$) and octahedral particles ($\zeta \rightarrow 2$), it is easier for cubic particles to form columnar phases than for octahedral particles. That is why the distribution change with $\zeta < 1.0$ is much more significant than that with $\zeta > 1.0$.

4.4. Fabric anisotropy

Anisotropy is one of the most important characteristics of granular materials [30–32]. The non-uniform distributions of particle orientations in the previous section intuitively reveal granular anisotropy to some extent. For a further quantitative investigation, the fabric tensor is introduced to quantify the fabric, given as [64]

$$\Phi = \frac{1}{N} \sum_{k=1}^N \mathbf{n}_k \cdot \mathbf{n}_k^T \quad (13)$$

where \mathbf{n}_k is the k th unit fabric vector, N the amount of all fabric vectors. Such a definition yields a 3 by 3 matrix with three eigenvalues ($\lambda_1 \geq \lambda_2 \geq \lambda_3$) and three eigenvectors. The eigenvalues and eigenvectors determine the magnitude and direction of the anisotropy, respectively. The deviatoric eigenvalue λ_d [65] given by Eq. (14), is used to determine the magnitude of anisotropy, considering all the three eigenvalues of the fabric tensor. Note that the larger the deviatoric eigenvalue λ_d is, the more anisotropic the fabric vectors.

$$\lambda_d = \frac{1}{\sqrt{2}} \sqrt{(\lambda_1 - \lambda_2)^2 + (\lambda_1 - \lambda_3)^2 + (\lambda_2 - \lambda_3)^2} \quad (14)$$

Three types of fabric vectors, i.e., particle orientation, contact normal and branch vector, are focused on. The particle orientation is along the major axis as mentioned previously. The contact normal is the contact direction (more details in Section 2.4). The branch vector is defined as the vector joining the centroids of two particles in contact.

It is evident that particle shape has a significant effect on fabric anisotropy as shown in Fig. 13. In detail, aspect ratio is more pronounced for oblate particles, compared with blockiness. With respect to anisotropy of particle orientations in Fig. 13 (a), it is more sensitive to blockiness for $\zeta < 1$, where $\zeta = 0.5$ shows the lowest anisotropy consistent with distributions of particle orientations in Fig. 12. Moreover, as shown in Fig. 13 (b), anisotropy of contact normals shows a similar relationship as mean coordination number Z with aspect ratio η , where the aspect ratios at the two peaks are near 0.4 and 2.0, slightly different from that of Z - η curves. Indeed, such a trend is consistent with the analysis in terms of probability distributions of coordination number in Section 4.2. This suggests that anisotropy of normal contacts correlates to mean coordination number more than packing density, implying that coordination number is able to reveal more particle-scale details than packing density, as mentioned in Section 4.2. Interestingly, anisotropy of branch vectors, referring to Fig. 13 (c), is almost twice less than that of particle orientations and contact normals, indicating that the distribution of branch vectors is more uniform than that of particle orientations and contact normals. That is to say, branch vectors are less dependent on particle shape than particle orientations and contact normals are. One direct explanation is that branch vectors are not sensitive to particle rotation. For example, the branch vector keeps constant if a particle rotates around its centroid without translation. A similar M-type trend between anisotropy of branch vectors and aspect ratio is observed. However, a small peak occurs at $\eta \simeq 1.0$, showing

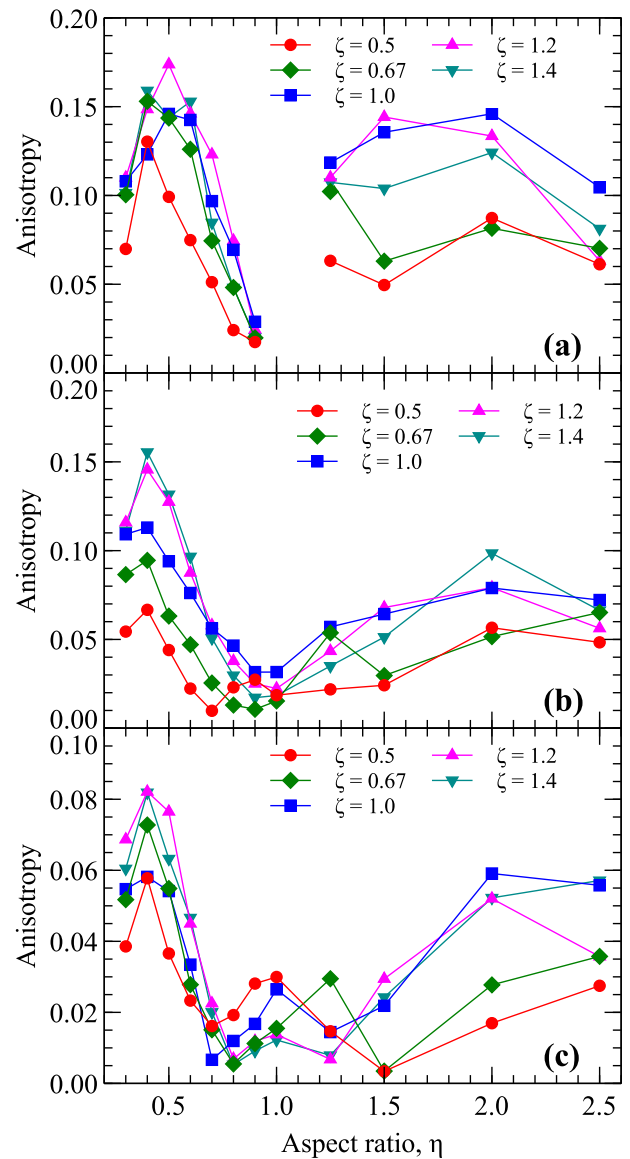


Fig. 13. Anisotropy of fabric vectors: (a) particle orientation; (b) contact normal; and (c) branch vector. Note: no data for particle orientations at $\eta = 1.0$ are presented.

that particle shape with $\eta = 1.0$ (i.e., superball) is not always corresponding to a low-anisotropic fabric.

The contribution of blockiness ζ to fabric anisotropy is related to aspect ratio η , although these two shape descriptors are defined individually. No clear relationship between anisotropy and blockiness is observed in Fig. 13. Nevertheless, for $\eta < 0.7$, anisotropy increases as blockiness increases; for $\eta > 1.25$, anisotropy decreases as blockiness decreases or increases from 1.0. For $\eta \simeq 1.0$, blockiness has an insignificant contribution to the anisotropy of both particle orientations and contact normals.

4.5. PDF of contact forces

Inter-particle contact forces play a vital role in force transmission within granular materials, forming contact force networks which have been recognized as the key factor determining the macroscopic mechanical properties of granular materials [66]. Nevertheless, it is challenging to characterize the contact network due to its spatial inhomogeneity [67,68]. Here emphasis is put on an important and

common quantity, the probability distribution function (PDF) of contact forces, for quantifying the contact network [50,67,69,70].

As shown in Fig. 14, PDF(F/\bar{F}) has a significant linear relationship with F/\bar{F} in log-linear scale, indicating that F/\bar{F} has an exponential probability distribution. In detail, contact forces at a range of [0.1, 7] times the average \bar{F} have a major proportion of up to 79%, forming strong contact force chains in the assembly; small forces less than $0.1\bar{F}$ exhibit a proportion of 20% or so, contributing to weak contact force chains; less than 1% of contact forces is greater than $7\bar{F}$. A similar feature was reported in the literature (e.g., [50,67,69,71]). However, a peak or plateau at around $F/\bar{F} = 1$ was observed in these literature where external load was performed on assemblies. It is not a surprise to have such a difference because the PDF of contact forces is history dependent [50]. In this work, particles experience force free settling under a gravitational field to reach an equilibrium state (i.e., jamming transmission). At this state, many contacts show small contact forces due to insignificant self weight applied. Based on this state, adding external load will make those weak contact force chains stronger, thereby reducing the proportion of small contact forces, which is the case in the literature.

With respect to the effect of particle shape, it is clear that the PDF of normalized contact forces keeps an almost constant distribution regardless of particle shape (i.e., aspect ratio η and blockiness ζ). That is to say, contact forces normalized by the average obey a particle-shape-independent distribution to some degree. However, it can be seen that particle shape has a more or less effect on the proportion of larger contact forces, e.g., $F/\bar{F} > 5.0$. It is worth pointing out that the present insignificant effect of particle shape is limited to the special case of packing under a gravitational field forming a relatively low stress state. Particle shape may give more contribution to the PDF (F/\bar{F}) of an assembly with a high stress state. This will be investigated in our future work.

5. Summary and conclusions

A superellipsoidal DEM model was developed to investigate random packing of monodisperse superellipsoidal particles with a broad range of shapes. Two shape descriptors (i.e., aspect ratio η and blockiness ζ) were used to control a particle shape. We examined the

effect of particle shape on fabric of a granular packing, and obtained some interesting results summarized as follows: (1) The relationship between packing density ϕ and aspect ratio η shows a M-type curve for ellipsoids. Changing blockiness ζ away from 1.0, the ϕ - η curve moves up seeing a M-type transferring to an inverted V-type trend for superellipsoids. Ellipsoids have the lowest packing density in the family of superellipsoids. (2) The mean coordination number Z increases to a peak, then slowly decreases as aspect ratio η increases or decreases from 1.0 for a given blockiness ζ . The corresponding distribution peak of coordination number is at a narrower range with different aspect ratios as blockiness ζ varies away from 1.0. (3) The distribution of particle orientations on the horizontal plane is much more uniform than that on the vertical plane. Moreover, major particles have orientations near the horizontal. Furthermore, the distribution is much more sensitive to blockiness than aspect ratio. (4) Anisotropy of both particle orientations and contact normals shows a similar M-type relationship with aspect ratio, two times larger than that of branch vectors. No clear relationship between anisotropy and blockiness is observed. (5) Contact forces normalized by the average obey such a clear exponential distribution that is particle-shape independent to some degree.

Acknowledgments

The authors appreciate the support of State Key Laboratory of Subtropical Building Science, SCUT (2014ZA03), Water Conservancy Science and Technology Innovation Project of Guangdong Province (2015-17), and the Science and Technology Project of POWERCHINA Huadong Engineering Corporation Limited (SD2013-10). The China Scholarship Council is greatly appreciated for financially supporting S. Zhao to study at Oregon State University.

Appendix A. Geometric quantities of a superellipsoid

Volume of a superellipsoid is given by

$$V = 2AB \left(\frac{1}{2} \epsilon_1 + 1, \epsilon_1 \right) B \left(\frac{1}{2} \epsilon_2, \frac{1}{2} \epsilon_2 \right) \quad (\text{A.1})$$

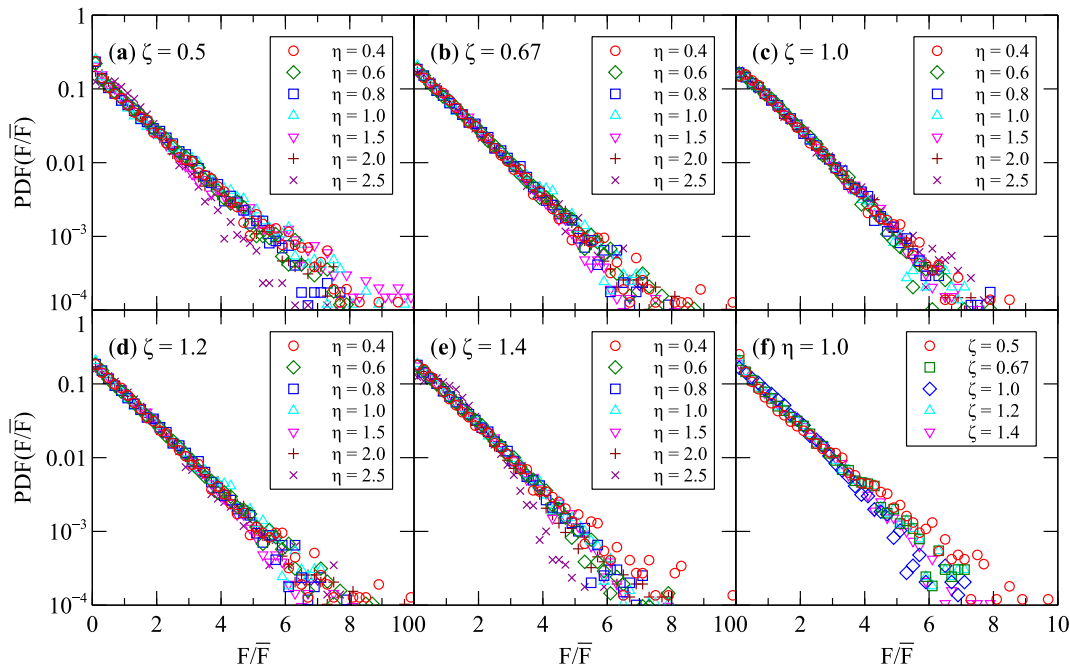


Fig. 14. Probability distribution functions (PDFs) of contact force F normalized by the average \bar{F} .

where A is short for $\frac{4}{3}abc\epsilon_1\epsilon_2$; the term $B(x,y)$ is a beta function related to gamma function and defined as

$$B(x,y) = 2 \int_0^{\pi/2} \sin^{2x-1} \phi \cos^{2y-1} \phi d\phi = \frac{\Gamma(x)\Gamma(y)}{\Gamma(x+y)} \quad (\text{A.2})$$

The principal moments of inertia of a superellipsoid are determined by

$$\begin{cases} I_1 = I_{xx} = \frac{1}{2}\rho A(b^2\beta_1 + 4c^2\beta_2) \\ I_2 = I_{yy} = \frac{1}{2}\rho A(a^2\beta_1 + 4c^2\beta_2) \\ I_3 = I_{zz} = \frac{1}{2}\rho A(a^2 + b^2)\beta_1 \end{cases} \quad (\text{A.3})$$

in which ρ is material density, and β_1 and β_2 are given as

$$\begin{cases} \beta_1 = B\left(\frac{3}{2}\epsilon_2, \frac{1}{2}\epsilon_2\right) B\left(\frac{1}{2}\epsilon_1, 2\epsilon_1 + 1\right) \\ \beta_2 = B\left(\frac{1}{2}\epsilon_2, \frac{1}{2}\epsilon_2 + 1\right) B\left(\frac{3}{2}\epsilon_1, \epsilon_1 + 1\right) \end{cases} \quad (\text{A.4})$$

Given a normal vector (n_x, n_y, n_z) on the surface, the corresponding local spherical coordinate (θ, ϕ) is obtained through the following function f :

$$\begin{cases} \theta = \text{atan2}\left(\text{Sign}(n_y)|bn_y|^{\frac{1}{2-\epsilon_1}}, \text{Sign}(n_x)|an_x|^{\frac{1}{2-\epsilon_1}}\right) \\ \phi = \text{atan2}\left(\text{Sign}(n_z)|cn_z|\cos(\theta)|^{2-\epsilon_2}, |an_x|^{\frac{1}{2-\epsilon_2}}\right) \end{cases} \quad (\text{A.5})$$

where the term $\text{atan2}(x,y)$ is the arctangent function of $\frac{x}{y}$ producing results in the range $(-\pi, \pi]$; the term $\text{Sign}(x)$ is the signum function defined as

$$\text{Sign}(x) = \begin{cases} -1 & \text{if } x < 0, \\ 0 & \text{if } x = 0, \\ 1 & \text{if } x > 0. \end{cases} \quad (\text{A.6})$$

Given the local spherical coordinate (θ, ϕ) of a point on the surface, the corresponding local Cartesian coordinate (x,y,z) is expressed via the following function F :

$$\begin{cases} x = \text{Sign}(\cos(\theta))a|\cos(\theta)|^{\epsilon_1}|\cos(\phi)|^{\epsilon_2} \\ y = \text{Sign}(\sin(\theta))b|\sin(\theta)|^{\epsilon_1}|\cos(\phi)|^{\epsilon_2} \\ z = \text{Sign}(\sin(\phi))c|\sin(\phi)|^{\epsilon_2} \end{cases} \quad (\text{A.7})$$

References

- [1] F.H. Stillinger, T.A. Weber, Packing structures and transitions in liquids and solids, *Science* 225 (4666) (1984) 983–989.
- [2] O. Pouliquen, M. Nicolas, P.D. Weidman, Crystallization of non-Brownian spheres under horizontal shaking, *Phys. Rev. Lett.* 79 (19) (1997) 3640–3643.
- [3] S.C. Glotzer, M.J. Solomon, Anisotropy of building blocks and their assembly into complex structures, *Nat. Mater.* 6 (8) (2007) 557–562.
- [4] A. Jaoshvili, A. Esakia, M. Porrati, P.M. Chaikin, Experiments on the random packing of tetrahedral dice, *Phys. Rev. Lett.* 104 (18) (2010) 185501.
- [5] J.D. Bernal, A geometrical approach to the structure of liquids, *Nature* 183 (4655) (1959) 141–147.
- [6] G.D. Scott, Radial distribution of the random close packing of equal spheres, *Nature* 194 (4832) (1962) 956–957.
- [7] J.L. Finney, Random packings and the structure of simple liquids. I. The geometry of random close packing, *Proc. R. Soc. Lond. A Math. Phys. Sci.* 319 (1539) (1970) 479–493.
- [8] A. Donev, I. Cisse, D. Sachs, E.A. Variano, F.H. Stillinger, R. Connelly, S. Torquato, P.M. Chaikin, Improving the density of jammed disordered packings using ellipsoids, *Science* 303 (5660) (2004) 990–993.
- [9] J. Baker, A. Kudrolli, Maximum and minimum stable random packings of platonic solids, *Phys. Rev. E* 82 (6) (2010) 061304.
- [10] P.A. Cundall, O.D.L. Strack, A discrete numerical model for granular assemblies, *Géotechnique* 29 (1) (1979) 47–65.
- [11] C.R. Abreu, F.W. Tavares, M. Castier, Influence of particle shape on the packing and on the segregation of spherocylinders via Monte Carlo simulations, *Powder Technol.* 134 (1) (2003) 167–180.
- [12] B.D. Lubachevsky, F.H. Stillinger, Geometric properties of random disk packings, *J. Stat. Phys.* 60 (5–6) (1990) 561–583.
- [13] L.K. Roth, H.M. Jaeger, Optimizing packing fraction in granular media composed of overlapping spheres, *Soft matter* 12 (4) (2016) 1107–1115.
- [14] H.P. Zhu, Z.Y. Zhou, R.Y. Yang, A.B. Yu, Discrete particle simulation of particulate systems: a review of major applications and findings, *Chem. Eng. Sci.* 63 (23) (2008) 5728–5770.
- [15] A. Wouterse, S.R. Williams, A.P. Philipse, Effect of particle shape on the density and microstructure of random packings, *J. Phys. Condens. Matter* 19 (40) (2007) 406215.
- [16] A.V. Kyrilyuk, A.P. Philipse, Effect of particle shape on the random packing density of amorphous solids, *Phys. Status Solidi (a)* 208 (10) (2011) 2299–2302.
- [17] A.G. Athanasiadis, M.Z. Miskin, P. Kaplan, N. Rodenberg, S.H. Lee, J. Merritt, E. Brown, J. Amend, H. Lipson, H.M. Jaeger, Particle shape effects on the stress response of granular packings, *Soft Matter* 10 (1) (2013) 48–59.
- [18] S. Li, J. Zhao, P. Lu, Y. Xie, Maximum packing densities of basic 3D objects, *Chin. Sci. Bull.* 55 (2) (2010) 114–119.
- [19] P. Lu, S. Li, J. Zhao, L. Meng, A computational investigation on random packings of sphere-spherocylinder mixtures, *Sci. China Phys. Mech. Astron.* 53 (12) (2010) 2284–2292.
- [20] X.L. Deng, R.N. Davé, Dynamic simulation of particle packing influenced by size, aspect ratio and surface energy, *Granul. Matter* 15 (4) (2013) 401–415.
- [21] W. Nan, Y. Wang, Y. Ge, J. Wang, Effect of shape parameters of fiber on the packing structure, *Powder Technol.* 261 (2014) 210–218.
- [22] Z. Zhou, R. Zou, D. Pinson, A. Yu, Dynamic simulation of the packing of ellipsoidal particles, *Ind. Eng. Chem. Res.* 50 (16) (2011) 9787–9798.
- [23] J. Gan, A. Yu, Z. Zhou, DEM simulation on the packing of fine ellipsoids, *Chem. Eng. Sci.* 156 (2016) 64–76.
- [24] Y. Jiao, S. Torquato, Maximally random jammed packings of platonic solids: hyperuniform long-range correlations and isotaticity, *Phys. Rev. E* 84 (4) (2011) 041309.
- [25] S. Torquato, Y. Jiao, Dense packings of polyhedra: platonic and Archimedean solids, *Phys. Rev. E* 80 (4) (2009) 041104.
- [26] J.H. Conway, S. Torquato, Packing, tiling, and covering with tetrahedra, *Proc. Natl. Acad. Sci.* 103 (28) (2006) 10612–10617.
- [27] J. Zhao, S. Li, W. Jin, X. Zhou, Shape effects on the random-packing density of tetrahedral particles, *Phys. Rev. E* 86 (3) (2012) 031307.
- [28] S. Zhao, X. Zhou, W. Liu, C. Lai, Random packing of tetrahedral particles using the polyhedral discrete element method, *Particuology* 23 (2015) 109–117.
- [29] J. Fonseca, C. O'Sullivan, M.R. Coop, P. Lee, Quantifying the evolution of soil fabric during shearing using directional parameters, *Géotechnique* 63 (6) (2013) 487–499.
- [30] E.S. Hosseininia, Investigating the micromechanical evolutions within inherently anisotropic granular materials using discrete element method, *Granul. Matter* 14 (4) (2012) 483–503.
- [31] J. Arthur, B. Menzies, Inherent anisotropy in a sand, *Géotechnique* 22 (1) (1972) 115–128.
- [32] F. Alonso-Marroquin, S. Luding, H. Herrmann, I. Vardoulakis, Role of anisotropy in the elastoplastic response of a polygonal packing, *Phys. Rev. E* 71 (5) (2005) 051304.
- [33] J.M. Duncan, Anisotropy and stress reorientation in clay, *J. Soil Mech. Found. Div.* 92 (ASCE# 4903 Proceeding) (1966)
- [34] A. Saada, G. Bianchini, Strength of one dimensionally consolidated clays, *J. Geotech. Geoenviron. Eng.* 101 (ASCE# 11707 Proceeding) (1975)
- [35] M. Oda, Fabrics and their effects on the deformation behaviors of sand, *Special Issue, Department of Foundation Engineering, Faculty of Engineering, Saitama University, Japan, 1977, p1–59.*
- [36] L. Yi, K. Dong, R. Zou, A. Yu, Radical tessellation of the packing of spheres with a log-normal size distribution, *Phys. Rev. E* 92 (3) (2015) 032201.
- [37] P. Richard, L. Oger, J. Troadec, A. Gervois, A model of binary assemblies of spheres, *Eur. Phys. J. E* 6 (4) (2001) 295–303.
- [38] J.G. Puckett, F. Lechenault, K.E. Daniels, Local origins of volume fraction fluctuations in dense granular materials, *Phys. Rev. E* 83 (4) (2011) 041301.
- [39] V. Luchnikov, N. Medvedev, L. Oger, J.-P. Troadec, Voronoi-Delaunay analysis of voids in systems of nonspherical particles, *Phys. Rev. E* 59 (6) (1999) 7205.
- [40] A. Baule, R. Mari, L. Bo, L. Portal, H.A. Makse, Mean-field theory of random close packings of axisymmetric particles, *Nat. Commun.* 4 (2013)
- [41] F.M. Schaller, M. Neudecker, M. Saadatfar, G.W. Delaney, G.E. Schröder-Turk, M. Schröder, Local origin of global contact numbers in frictional ellipsoid packings, *Phys. Rev. Lett.* 114 (15) (2015) 158001.
- [42] K. Dong, C. Wang, A. Yu, Voronoi analysis of the packings of non-spherical particles, *Chem. Eng. Sci.* 153 (2016) 330–343.
- [43] P.W. Cleary, N. Stokes, J. Hurley, Efficient collision detection for three dimensional super-ellipsoidal particles, *Proceedings of 8th International Computational Techniques and Applications Conference CTAC97, Adelaide, 1997,*
- [44] J.R. Williams, A.P. Pentland, Superquadrics and modal dynamics for discrete elements in interactive design, *Eng. Comput.* 9 (2) (1992) 115–127.
- [45] P.W. Cleary, Large scale industrial DEM modelling, *Eng. Comput.* 21 (2/3/4) (2004) 169–204.
- [46] J. Kozićki, F. Donzé, Yade-open dem: an open-source software using a discrete element method to simulate granular material, *Eng. Comput.* 26 (7) (2009) 786–805.

- [47] V. Šmilauer, E. Catalano, B. Chareyre, S. Dorofeenko, J. Duriez, A. Gladky, J. Kozicki, C. Modenese, L. Scholtès, L. Sibille, et al. Yade reference documentation, 2010, <http://yade-dem.org/doc/>.
- [48] A.H. Barr, Superquadrics and angle-preserving transformations, *IEEE Comput. Graph. Appl.* 1 (1) (1981) 11–23.
- [49] M.P. Allen, D.J. Tildesley, *Computer Simulation of Liquids*, Oxford University Press, 1989.
- [50] K. Bagi, Statistical analysis of contact force components in random granular assemblies, *Granul. Matter* 5 (1) (2003) 45–54.
- [51] K. Johnson, *Contact Mechanics*, Cambridge University Press, London, 1985.
- [52] C. Wellmann, C. Lillie, P. Wriggers, A contact detection algorithm for superellipsoids based on the common-normal concept, *Eng. Comput.* 25 (5) (2008) 432–442.
- [53] J.C. Lagarias, J.A. Reeds, M.H. Wright, P.E. Wright, Convergence properties of the Nelder–Mead simplex method in low dimensions, *SIAM J. Optim.* 9 (1) (1998) 112–147.
- [54] G.v.d. Bergen, Efficient collision detection of complex deformable models using AABB trees, *J. Graphics Tools* 2 (4) (1997) 1–13.
- [55] P.W. Cleary, The effect of particle shape on simple shear flows, *Powder Technol.* 179 (3) (2008) 144–163.
- [56] P.W. Cleary, G.G. Pereira, V. Lemiale, C. Delle Piane, M.B. Clennell, Multiscale model for predicting shear zone structure and permeability in deforming rock, *Computational Particle Mechanics* 3 (2) (2016) 179–199.
- [57] G.-C. Cho, J. Dodds, J.C. Santamarina, Particle shape effects on packing density, stiffness, and strength: natural and crushed sands, *J. Geotech. Geoenviron. Eng.* 132 (5) (2006) 591–602.
- [58] Y.F. Cheng, S.J. Guo, H.Y. Lai, Dynamic simulation of random packing of spherical particles, *Powder Technol.* 107 (1–2) (2000) 123–130.
- [59] L.F. Liu, Z.P. Zhang, A.B. Yu, Dynamic simulation of the centripetal packing of mono-sized spheres, *Physica A* 268 (3–4) (1999) 433–453.
- [60] G.W. Delaney, P.W. Cleary, The packing properties of superellipsoids, *Europhys. Lett.* 89 (3) (2010) 34002.
- [61] Y. Jiao, F. Stillinger, S. Torquato, Optimal packings of superballs, *Phys. Rev. E* 79 (4) (2009) 041309.
- [62] I. Agnolin, J.-N. Roux, Internal states of model isotropic granular packings. III. Elastic properties, *Phys. Rev. E* 76 (6) (2007) 061304.
- [63] S. Zhao, X. Zhou, W. Liu, Discrete element simulations of direct shear tests with particle angularity effect, *Granul. Matter* 17 (6) (2015) 793–806.
- [64] M. Satake, Fabric tensor in granular materials, *Proc., IUTAM Symp. on Deformation and Failure of Granular materials*, Delft, The Netherlands, 1982.
- [65] D. Barreto, C. O'Sullivan, L. Zdravkovic, Quantifying the evolution of soil fabric under different stress paths, *Powders and Grains 2009: Proceedings of the 6th International Conference on Micromechanics of Granular Media*, 1145, AIP Publishing, 2009, pp. 181–184.
- [66] F. Radjai, D.E. Wolf, M. Jean, J.-J. Moreau, Bimodal character of stress transmission in granular packings, *Phys. Rev. Lett.* 80 (1) (1998) 61.
- [67] T.S. Majmudar, R.P. Behringer, Contact force measurements and stress-induced anisotropy in granular materials, *Nature* 435 (7045) (2005) 1079–1082.
- [68] S. Ostoic, E. Somfai, B. Nienhuis, Scale invariance and universality of force networks in static granular matter, *Nature* 439 (7078) (2006) 828–830.
- [69] E. Azéma, F. Radjai, R. Peyroux, G. Saussine, Force transmission in a packing of pentagonal particles, *Phys. Rev. E* 76 (1) (2007) 011301.
- [70] E. Azéma, F. Radjai, Force chains and contact network topology in sheared packings of elongated particles, *Phys. Rev. E* 85 (3) (2012) 031303.
- [71] W.L. Vargas, J.J. McCarthy, Thermal expansion effects and heat conduction in granular materials, *Phys. Rev. E* 76 (4) (2007) 041301.